Microwave Hydrothermal Renovating and Reassembling Spent Lithium Cobalt Oxide for Lithium-ion Battery

Yang Liu [1], Hongjian Yu [1], Yue Wang [1], Dan Tang [1], Weixin Qiu [1], Wenzhang Li [1, 2, *], Jie Li [1, *]

[1]*School of Chemistry and Chemical Engineering, Central South University, Changsha, 410083, China*

[2] *Hunan Provincial Key Laboratory of Chemical Power Sources, Central South University, Changsha, 410083, China*

Corresponding author: liwenzhang@csu.edu.cn; lijieliu@csu.edu.cn.

Abstract

With the growing number of lithium-ion batteries (LIBs) that are consumed by worldwide people, recycling is necessary for addressing environmental problems and alleviating energy crisis. Especially, it is meaningful to regenerate LIBs from spent batteries. In this paper, the microwave hydrothermal method is used to replenish lithium, assemble particles and optimize the crystal structure of the spent lithium cobalt oxide. The microwave hydrothermal process can shorten the reaction time, improve the internal structure, and uniformize the particle size distribution of lithium cobalt oxide. It helps to construct a regenerated lithium cobalt oxide ($LiCoO_2$) battery with high-capacity and high-rate properties (141.7 mAh g^{-1} at 5C). The cycle retention rate is 94.5% after 100 cycles, which is far exceeding the original lithium cobalt oxide (89.7%) and $LiCoO_2$ regenerated by normal hydrothermal method (88.3%). This work demonstrates the feasibility to get lithium cobalt oxide batteries with good structural stability from spent lithium cobalt oxide batteries.

Keywords: Spent lithium cobalt oxide; Recycle, Regenerated battery; Stability; Microwave hydrothermal method

1. Introduction

Lithium cobalt oxide ($LiCoO_2$) is one of the cathode materials that are employed in commercial Li-ion batteries (Lin et al., 2021; Lyu et al., 2021). In the past years, the recycling of cathode compounds attracts a lot of attention due to the high price of Co and Li as well as the target of resource sustainability(Bai et al., 2020; Lahtinen et al., 2021; Natarajan and Aravindan, 2018; Wang et al., 2020; Ye et al., 2021). There are several methods reported by numerous researchers to recycle spent lithium-ion batteries (LIBs), such as pyrometallurgical (Makuza et al., 2021), hydrometallurgical (Chen et al., 2019; dos Santos et al., 2019; Li et al., 2021; Wang et al., 2021; Zhou et al., 2021a; Zhou et al., 2020), direct recovery methods (Chen et al., 2016; Shi et al., 2018; Zhang et al., 2014), physical methods (Yu et al., 2018), etc.

For the pyrometallurgical process, the LIBs are smelted in a furnace. In the process, the organic materials (such as separator and plastic) are burned away, and the anode (carbon) is not only the fuel to keep the temperature of the furnace but also a reducing agent to reduce metal oxide cathode (Ren et al., 2017). The chemical reactions are fast so that a large treating capacity is easy to be achieved in the industry (Makuza et al., 2021). Sometimes, the waste LIBs as a kind of metal ore was introduced in the traditional pyrometallurgical process. But it also has some drawbacks that need to be addressed, such as CO_2 evolution, formation of fluoride and high energy consumption. Besides, further separation is still needed to get pure materials from the as-prepared alloys. The hydrometallurgical method can recycle the constituents at low temperatures(Wang et al., 2020). Numerous chemicals were employed as leaching agents, such as inorganic acid ($HCl+H_2O_2$(Guo et al., 2016), HNO_3, $H_2SO_4+H_2O_2$(Bertuol et al., 2016) and H_3PO_4(Chen et al., 2017)), organic acid (citric acid(dos Santos et al., 2019), DL-malic acid + H_2O_2(Zhou et al., 2021a), ascorbic acid(Li et al., 2012), and nitrilotriacetic acid(Nayaka et al.,

2019)) However, some of the unwanted elements (Al and Cu) were also leached in the solution, which increased the cost to get pure materials. After gaining the products of hydrothermal methods, some researchers synthesized $LiCoO_2$ cathodes (Wang et al., 2021). Additionally, electrolytic leaching (Zhou et al., 2021b), molten-salt-electrolysis(Zhang et al., 2019a), and "ammonium chloride roasting + water leaching"(Qu et al., 2020) were also used to leach Co based chemicals from the spent Li batteries, and the regenerated LIBs were constructed by calcining the mixture of Co chemicals and Li_2CO_3.

To shorten the process for reconstructing LIBs, researchers have demonstrated some direct recycling strategies in recent years. Before the treatment, the active materials were obtained by dismantling, electrode separation and purification. Because the element Li is not stoichiometry in the waste $LiCoO_2$, some researchers mixed and annealed a pre-determined amount of Li_2CO_3 with the waste $LiCoO_2$. The discharge capacity of regenerated LIBs is around 130 mAh g^{-1}(Gao et al., 2020; Sita et al., 2017). Nie et al. sieved the regenerated powers after annealing at 900 ℃ for 12 h, and the discharge capacity reaches 152.4 mAh g^{-1}(Nie et al., 2015). Meanwhile, Yang et al. used LiOH-KOH molten salt to repair $LiCoO_2$ and removed the impurities from the spent LIBs. The discharge capacity of regenerated LIBs was 149.1 mAh g^{-1}, and it was 138.7 mAh g^{-1} after 100 cycles(Yang et al., 2021). A discharge capacity of 144.5 mAh g^{-1} was also obtained for the $LiCoO_2$ battery regenerated by LiOH-KOH-$LiCO_3$ molten salt(Yang et al., 2020), but over amount of inorganic salt need to be washed away. The hydrothermal method followed by annealing is a nice method to replenish lithium in the spent Li_yCoO_x, which is flexible in feed materials without calculating the loss amount of lithium for the waste $LiCoO_2$. The initial discharge capacity of regenerated LIBs is 148.2 mAh g^{-1}, and it is 135.1 mAh g^{-1} after 100 cycles (Shi et al., 2018). An electrochemical relithiation method was also reported, and the discharge

capacity of regenerated LCO battery is 136 mAh g^{-1} (Zhang et al., 2020).

In recent years, the requirements for the capacity of LIBs are getting higher and higher. The discharge specific capacity of $LiCoO_2$ can be improved by increasing the charge cutoff voltage and increasing the amount of deintercalated lithium, but the cycle performance will deteriorate sharply. Therefore, a better structural stability is necessary for the $LiCoO_2$ LIBs under high voltage. The particle size of $LiCoO_2$ regenerated by the reported hydrothermal method was random, and the crystallinity had not been enhanced yet. Considering the fact that $LiCoO_2$ is an ionic crystal with strong polarity(Yu et al., 2018) and a possible candidate for microwave absorption(Yang et al., 2019a, b), it can be heated in the microwave hydrothermal method. Cheng et al. noted that dispersed $LiCoO_2$ nanosheets can be restacked into ordered $LiCoO_2$ (Cheng et al., 2016). It has been noted that the microwave hydrothermal method needs a shorter reaction time and lower experimental temperature than the traditional hydrothermal method, which has been confirmed for the replenishing lithium in $Li_{1+x}Mn_{1.5}Ni_{0.5}O_4$(Moorhead-Rosenberg et al., 2014). Besides, powders synthesized by the microwave hydrothermal method have high purity, good crystallinity and uniform microstructures. Thus, self-heating under microwave can lead to a high efficient heat field in and near the $LiCoO_2$ particles, which may affect the crystallinity of regenerated $LiCoO_2$. Thus, a regenerated $LiCoO_2$ with high capacity and great structural stability can be expected by using microwave hydrothermal method.

In the present work, we used a microwave hydrothermal method to regenerate $LiCoO_2$ materials from the waste Li_yCoO_x electrode of spent LIBs. The regenerated $LiCoO_2$ had uniform particle size distribution, and great structural stability was obtained. As a result, the constructed $LiCoO_2$ battery presents high capacity and high rate performance, which is 141.7 mAh g^{-1} at 5C.

2. Experimental Section

2.1 Dismantling, electrode separation

Commercial spent $LiCoO_2$ batteries (Guangdong Pinsheng Co std.) used in cell phones were bought from market. The waste battery was discharged at 0.1C (1 C=150 mAh g-1) between 3-4.3 V. To obtain the waste cathode materials, the spent LIBs were discharged and manually disassembled following the process in Fig. S1. The disassembled waste cathode strip was rinsed with dimethyl carbonate thoroughly, which was then dried and cut into 1 cm × 1 cm pieces. They were soaked in N-methyl-2-pyrrolidone for 30 min, and then ultrasonic treatment for 20 min. After centrifugation at 3500 rpm for 5 min, the precipitation was washed with deionized (DI) water and centrifugation several times. Finally, the waste $LiCoO_2$ powder was obtained after drying, which was recorded as LCOE. The powder was kept in a glass desiccator before the next step (regeneration or prepared into electrodes).

2.2 Regeneration of $LiCoO_2$

The regeneration process is achieved by a microwave hydrothermal method using a microwave hydrothermal reactor (XH-600, Beijing Xiang Hu Sci&Tech Development Co. Ltd). In typical, 2 g of LCOE powder is added into a 50 mL lithium hydroxide solution (4 M). The mixture was then transferred to a 100 mL microwave hydrothermal reactor. After treating at 220 ℃ for 30/45/60/120 min, the black powder was obtained after centrifugation, washing and drying, which is notated as M-30/45/60/120. The regenerated lithium cobalt oxide powder was annealed at 800 ℃ with a ramping rate of 5 ℃ min^{-1} in a tube furnace for 4 h, which was notated as AM-30/45/60/120. For comparison, the mixture of LCOE and 80 mL lithium hydroxide solution (4 M) was treated in a normal hydrothermal reactor at 220 ℃ for 4 h. The product is named as HLCOE,

and it is also annealed to get the product named as AHLCOE.

2.3 Structure characterization

Thermal field emission scanning electron microscopy (SEM, JSM-7610F) equipped with an energy dispersive spectroscopy was used to observe the microstructure and composition of the samples, and the operating voltage was 10 kV. The particle size was estimated by using the software ImageJ. Siemens D500 X-ray diffraction (XRD) was used to characterize the phase structure of the active material. The chemical state of Co was analyzed by X-ray photoelectron spectroscopy (XPS, K-Alpha 1063). The amounts of Li and Co were also confirmed by an inductively coupled plasma emission spectrometer (ICAP6300).

2.4 Electrochemical characterization

The process for preparing cathode and assembling battery was following the reported methods, and the details were also presented in the supporting information. The Land battery test system produced by Wuhan Land Electronics Co., Ltd. was used to test the charge and discharge of lithium-ion batteries. The test was performed at a constant temperature of 25 ℃. The battery is circulated at 1 C (1 C=150 mAh g^{-1}) between 3-4.3 V. The electrochemical impedance spectroscopy (EIS) was measured by CHI 760e in the frequency of 10 kHz-0.01 Hz.

3. Results and discussions

Fig.1 shows the XRD patterns of the above samples. In Figs. 1a-e, the peaks at 18.96, 37.44, 39.16, 45.26, 59.64 and 65.46 ° are related to the (003), (101), (012), (104), (107) and (018) planes of $LiCoO_2$ (PDF#50-0653). With the increase of microwave hydrothermal time, the ratio

of (003) and (104) peak is greater, and the ratio of AM-45 is larger than that of AHLCOE (Table S1). It demonstrates that the microwave hydrothermal process could promote the crystal growth to the layered structure with a certain reaction time (Shi et al., 2016). Fig. 1f is the partially enlarged view at 2θ of 43-49°. The samples regenerated by microwave hydrothermal method have smaller half-peak width of (104) peak compared to the AHLCOE. It indicates that the microwave hydrothermal process can promote the crystallization process of lithium cobalt oxide, and the $LiCoO_2$ layers should be stacked orderly. Figs. 1g-1i show the Co 2p XPS spectra of LCOE, HLCOE, and M-45. There seem two peaks in the plot of LCOE, which can be deconvolved and assigned to Co^{3+} (778.41 and 793.75 eV) and Co^{2+} (781.8 and 797.53 eV). For HLCOE, the two peaks can also be fitted into Co^{3+} (780.19 and 795.53 eV) and Co^{2+} (781.21 and 796.94 eV). It is also found that the ratio of Co^{3+}/Co^{2+} area increases to 1.39 (HLCOE) from 0.45 (LCOE), which is further increased to 2.60 for M-45. This indicates that the spent $LiCoO_2$ has been recovered, and microwave hydrothermal method presents a better result (Yang et al., 2020).

To compare the heating situation on lithium cobalt particles under microwave hydrothermal and ordinary hydrothermal methods, the COMSOL Multiphysics software was used to simulate with microwave heating (microwave hydrothermal method, Fig. 2a) and conductive heating (ordinary hydrothermal method, Fig. 2b), respectively. It can be found that the temperature distribution (Fig. S2) across the lithium cobalt oxide particle is more homogeneous in microwave hydrothermal method (Fig. 2c) than that in ordinary hydrothermal method (Fig. 2d). This is favor for lithium diffusion inside the particle, and it may be one of the reasons for the good crystallinity of samples treated by microwave hydrothermal method.

Fig. 3 shows the surface morphology of LCOE and regenerated LCO with normal and microwave hydrothermal methods. The LCOE (Fig. 3a) exhibits a polygonal structure with edges,

and some cracks can be seen on the surface of the particles (inset of Fig. 3a). After replenishing Li by traditional hydrothermal treatment and annealing, the cracks disappear (Fig. 3b). It can also be found that the AHLCOE keeps the polygonal structure, and some small particles adhere to the large particle. For LCO regenerated by microwave hydrothermal method, the cracks disappear (insets of Figs. 3c-f), and the amount of attached small particles decreases (Figs. 3c-f). The AM-45 presents a more homogeneous morphology than others, and its average particle size is about 13.38±1.74 μm (Fig. 4). With the extending microwave hydrothermal time, there are more particles with the size larger than 16 μm. It indicates that the extension of microwave hydrothermal time is beneficial to the growth of particles. According to the results of XRD patterns (Fig. 1) and SEM images (Fig. 3), the cracked and small lithium cobalt oxide particles are swallowed into the large particles (Fig. 5, the unit cell draw by using VESTA(Momma and Izumi, 2011)). But the heat in microwave hydrothermal method comes from the dipole rotation, and molecules will align themselves in the electromagnetic field. It helps to organize the $LiCoO_2$ layer into a more orderly stack compared to the conventional hydrothermal method (Cheng et al., 2016).

To confirm the replenishing amounts of lithium ion, the samples were dissolved and measured by inductively coupled plasma. As shown in Table 1, the ratio of Li and Co increase after microwave hydrothermal treatment, but it doesn't reach the ideal proportion (1.0) until the time is equal to or greater than 45 min. After further annealing, the Li/Co ratio slightly decrease. But it is still close to 1 for AM-45, AM-60 and AM-120.

In order to compare the charge-discharge performance, the first charge-discharge curves of lithium cobalt oxide regenerated with different microwave hydrothermal time are shown in Fig. 6a. There are a large platform at ~3.9 V and a small platform at 4.2 V caused by phase change

188 from hexagonal phase to monoclinic phase (Xue et al., 2018). It validates that the internal
189 structure of lithium cobalt oxide has been greatly improved after microwave hydrothermal
190 treatment, which enhances the reversibility of structure transform. It is noted that the discharge
191 capacity of AM-45 reaches 151.5 mAh g^{-1}, which is higher than that of AM-30. In addition, it
192 can be seen that the voltage drop is fast at the beginning of the discharge curve for AM-60 and
193 AM-120 (Fig. 6a). According to the results in Table 1, the low discharge specific capacities of
194 AM-60 and AM-120 are not caused by the absence of lithium ions, but due to the large particle
195 size of lithium cobalt oxide particles, which increases the diffusion distance of lithium ions and
196 leads to poor magnification performance.

197 Fig. 6b shows the cycle capacity curves of LCOE, commercial LCO, and regenerated
198 lithium cobalt oxide under 25 ℃, 1 C current density charge-discharge test, and the test voltage
199 range is 3.0-4.3 V. The initial discharge capacity of LCOE is only 108 mAh g^{-1}, and the capacity
200 decay obviously. The AHLCOE has an initial discharge capacity of ~152 mAh g^{-1}, which is
201 close to the commercial LCO. But the capacity of AHLCOE decay faster than that of commercial
202 LCO. For the LCO regenerated by microwave hydrothermal method, the curves of each sample
203 are gentle with a slow decay in capacity. It means that the high crystallinity provides high
204 stability for the charge-discharge cycle. The discharge specific capacity of AM-30 is less than
205 150 mAh g^{-1} because the Li has not been replenished yet until microwave hydrothermal reaction
206 for 45 min. The initial discharge capacity of AM-45 (151.5 mAh g^{-1}) is close to commercial LCO,
207 indicating that its capacity has almost been recovered completely. More interesting, the discharge
208 capacity is still up to 143.2 mAh g^{-1} after 100 cycles, and the cycle retention rate is as high as
209 94.5%, which is better than that of commercial lithium cobalt oxide (87.3%), AHLCOE (80.7%)
210 and most of the reported values about regenerated lithium cobalt oxide batteries (Table S2)(Chen

et al., 2016; Cheng et al., 2016; Fei et al., 2021; Lahtinen et al., 2021; Meng et al., 2018; Nie et al., 2015; Shi et al., 2018; Sita et al., 2017; Yang et al., 2020). When the microwave hydrothermal time reaches 60 min and 120 min, the sample also has high electrochemical stability. It exhibits a stable structure of LCO regenerated by microwave hydrothermal method, which leads to better cyclic stability.

Fig. 6c and 6d show the dQ/dV plots for the charge and discharge curves at first and 100 cycles. In Fig. 6c, the main oxidation and reduction peaks (p_1/p_1', p_2/p_2', and p_3/p_3') can be seen at around 3.93, 4.09, and 4.19 V in the curves of each sample. These peaks are related to the phase transitions (hexagonal phase → second hexagonal phase → monoclinic phase → third hexagonal phase in sequence)(Zhu et al., 2014). The hexagonal phase and second hexagonal phase occur at the potential around peaks p_1/p_1', and it is attributed to the transformation of Co^{3+}/Co^{4+}. The p_2/p_2' and p_3/p_3' peaks can be assigned to the transition between order and disorder structure (Wang et al., 1999). In Fig. 6e and 6f, there are neglected potential differences between the first cycle and 100 cycles in oxidation and reduction peaks for AM-30 and AM-45. But a notable difference can be seen for either AM-60 (Fig. 6g) or AM-120 (Fig. 6h), which means large polarization in the sample. This may be an explanation for the lower discharge capacity of AM-60 and AM-120 compared to AM-45(Cheng et al., 2020). In Fig. 6i, the intensities of p_1/p_1' peaks decrease for AHLCOE, which is a result of the degradation of $LiCoO_2$ (Dokko et al., 2000). Meanwhile, the p_2/p_2' and p_3/p_3' peaks are almost disappeared, indicating the serious cell polarization in AHLCOE after testing for 100 cycles.

The charge transfer ability was also studied by electrochemical impedance spectroscopy (EIS). In Fig. 7a, the Nyquist plots were compared for the batteries tested after 1 cycle at 0.05 C and 50 cycles at 1 C. There are two semicircles in the Nyquist plots of the batteries, which are

related to the resistance at the interface of electrode/electrolyte (R_{sp}) and charge transfer resistance (R_{ct}) (Fei et al., 2021). The resistance increases due to the formation of SEI film after multiple cycles. The series resistance is similar between AHLCOE(6.24 Ω) and AM-45(6.60 Ω). But the R_{sp}(9.75 Ω) and R_{ct}(18.49 Ω) of AM-45 are lower than those of AHLCOE (11.61 and 23.6 Ω, respectively). At the same time, AM-45 presents a higher Li^+ ion diffusion coefficient (2.81×10^{-11} cm^2/s, Fig. 7b, calculation details are shown in the supporting information) compared to AHLCOE (1.81×10^{-11} cm^2/s) (Zhang et al., 2019b). These results can explain the high discharge capacity in Fig. 6b.

Figs. 7c and 7d show the XRD patterns of AM-45, AHLCOE, and LCO after 100 cycles to study the changes in the crystal structure. In Fig. 7c, the I(003) / I(104) of AM-45 is still large after 100 cycles, and the peak splitting of (006)/(012) and (018)/(110) is obvious. It indicates that the ordered degree of the material is still high after cycling. In Fig. 7d, the half-peak width of AM-45 slightly increases to 0.12 after 100 cycles, which is smaller than that of commercial lithium cobalt oxide (0.13) and AHLCOE (0.20) after the similar cycle test. Besides, there is a peak at $2\theta\approx36.8^o$ for AHLCOE instead of AM-45 after 100 cycles, which belongs to (311) planes of cubic Co_3O_4 (PDF#42-1467). This may be one of the reasons for the poor stability of AHLCOE. Based on the above results, it can be found that the crystallinity and orderly internal structure can be maintained for LCO regenerated by microwave hydrothermal method, which is the main reason for the high stability of Li-ion battery.

Fig. 7e shows the cycle rate of the regenerated samples with different microwave hydrothermal time. It can be clearly seen that AM-45 has the highest discharge specific capacity and the best cycle rate at 0.5-5C. The discharge specific capacity at 0.1C is 153.8 mAh g^{-1}. The specific discharge capacity of 5 C is 141.7 mAh g^{-1}, which may be due to the orderly stacking of

257 $LiCoO_2$ layers. At the same time, the capacity retention rate at a high rate reaches 92.1%, which
258 is much higher than that of AHLCOE (89.7%), the commercial lithium cobalt oxide (88.3%) and
259 most of the reported values about regenerated lithium cobalt oxide batteries (Table S3)(Lahtinen
260 et al., 2021; Meng et al., 2018; Qu et al., 2020; Shi et al., 2018; Yang et al., 2020). According to
261 the results in Figs. 1, 3 and 7c, the monocrystalline-like lithium cobalt oxide particles
262 regenerated by microwave hydrothermal process has higher discharge capacity at high current
263 density, because it can improve the internal structure of lithium cobalt oxide and increase the
264 diffusion rate of lithium ions(Cheng et al., 2021; Cheng et al., 2020; Jena et al., 2019; Lyu et al.,
265 2021). However, when the microwave hydrothermal time reaches 60 min, the capacity drops
266 sharply to 135.6 mAh g^{-1} at 0.5 C. This is due to the longer lithium ion diffusion path and slower
267 Li-ion transfer rate that results from the overgrowth of the particle under long microwave
268 hydrothermal time (Wu et al., 2016). In addition, the diffusion rate of lithium ions has little effect
269 on the capacity at a small current, but the concentration difference and diffusion polarization of
270 embedded ions increase at a large current, so the capacity decreases obviously. To quantify the
271 polarization and quantitatively study the effect of microwave hydrothermal time on the material,
272 Fig. 7f specifies the average difference of charge-discharge voltage for each sample. The smaller
273 difference means the better the electronic conductivity and Li^+ conductivity, and the less the
274 polarization it will be (Shi et al., 2018). It can be found that the voltage difference of AM-60 and
275 AM-120 at each charge-discharge rate is much larger than that of other samples. This is mainly
276 caused by the larger crystal particles and the longer internal lithium ion diffusion path, which is
277 consistent with the above description. The AM-45 has the lowest charging-discharge voltage
278 difference, and the voltage difference is only 0.107 V at 5 C, which is much smaller than that of
279 the regenerated samples by ordinary hydrothermal method (0.152 V) and the original lithium

cobalt oxide (0.150 V). It is further proved that the microwave hydrothermal process can enhance the electron conductivity and Li^+ conductivity of regenerated lithium cobalt oxide, and greatly reduce the internal polarization of the material. These characteristics lead to high capacity and high rate performance.

4. Conclusion

In this work, the spent lithium cobalt oxide (LCO) is regenerated by a microwave hydrothermal method in a short time. The lithium ions can be completed replenished in 45 min using microwave hydrothermal method, and the small and cracked waste LCO particles were assembled into large particles with uniform particle size, leading to an improved crystallinity compared to the traditional hydrothermal method. More interesting, the constructed $LiCoO_2$ battery presents high capacity and high rate performance due to the orderly structure, which is 141.7 mAh g^{-1} at 5C. This paper provides a strategy to renovate and regenerate the waste cathode material with high capacity and high stability without additional doping or surface coating.

Acknowledgements

This study was supported by the National Nature Science Foundation of China (21878340), the Hunan Provincial Science and Technology Plan Project of China (No. 2017TP1001), and Hunan Provincial Natural Science Foundation of China (No. 2020JJ5693). Liu thanks for the free source code of software (ImageJ) of Wayne Rasband (wayne@codon.nih.gov, Research Services Branch, National Institute of Mental Health, Bethesda, Maryland, USA). Liu thanks for the suggestions from Lei Ming (School of Metallurgy and Environment, Central South University).

References

Bai, Y., Muralidharan, N., Li, J., Essehli, R., Belharouak, I., 2020. Sustainable Direct Recycling of Lithium-Ion Batteries via Solvent Recovery of Electrode Materials. ChemSusChem 13, 5664-5670. https://doi.org/10.1002/cssc.202001479.

Bertuol, D.A., Machado, C.M., Silva, M.L., Calgaro, C.O., Dotto, G.L., Tanabe, E.H., 2016. Recovery of cobalt from spent lithium-ion batteries using supercritical carbon dioxide extraction. Waste Management 51, 245-251. https://doi.org/10.1016/j.wasman.2016.03.009.

Chen, S., He, T., Lu, Y., Su, Y., Tian, J., Li, N., Chen, G., Bao, L., Wu, F., 2016. Renovation of $LiCoO_2$ with outstanding cycling stability by thermal treatment with Li_2CO_3 from spent Li-ion batteries. Journal of Energy Storage 8, 262-273. https://doi.org/10.1016/j.est.2016.10.008.

Chen, X., Kang, D., Cao, L., Li, J., Zhou, T., Ma, H., 2019. Separation and recovery of valuable metals from spent lithium ion batteries: Simultaneous recovery of Li and Co in a single step. Separation and Purification Technology 210, 690-697. https://doi.org/10.1016/j.seppur.2018.08.072.

Chen, X., Ma, H., Luo, C., Zhou, T., 2017. Recovery of valuable metals from waste cathode materials of spent lithium-ion batteries using mild phosphoric acid. Journal of Hazardous Materials 326, 77-86. https://doi.org/10.1016/j.jhazmat.2016.12.021.

Cheng, L., Zhang, B., Su, S.-L., Ming, L., Zhao, Y., Tan, X.-X., 2021. Highly ordered structure in single-crystalline $LiNi_{0.65}Co_{0.15}Mn_{0.20}O_2$ with promising Li-ion storage property by precursor pre-oxidation. Journal of Solid State Chemistry 297, 122045. https://doi.org/10.1016/j.jssc.2021.122045.

Cheng, L., Zhang, B., Su, S.-L., Ming, L., Zhao, Y., Wang, C.-H., Ou, X., 2020. Comparison of monocrystalline and secondary LiNi0.5Co0.2Mn0.3O2 cathode material for high-performance lithium-ion batteries. Journal of Alloys and Compounds 845, 156202. https://doi.org/10.1016/j.jallcom.2020.156202.

Cheng, Q., Yang, T., Li, Y., Li, M., Chan, C.K., 2016. Oxidation–reduction assisted exfoliation of $LiCoO_2$ into nanosheets and reassembly into functional Li-ion battery cathodes. Journal of Materials Chemistry A 4, 6902-6910. 10.1039/C5TA09069E.

Dokko, K., Horikoshi, S., Itoh, T., Nishizawa, M., Mohamedi, M., Uchida, I., 2000. Microvoltammetry for cathode materials at elevated temperatures: electrochemical stability of single particles. Journal of Power Sources 90, 109-115. https://doi.org/10.1016/S0378-7753(00)00456-0.

dos Santos, C.S., Alves, J.C., da Silva, S.P., Evangelista Sita, L., da Silva, P.R.C., de Almeida, L.C., Scarminio, J., 2019. A closed-loop process to recover Li and Co compounds and to resynthesize $LiCoO_2$ from spent mobile phone batteries. Journal of Hazardous Materials 362, 458-466. https://doi.org/10.1016/j.jhazmat.2018.09.039.

Fei, Z., Zhang, Y., Meng, Q., Dong, P., Fei, J., Zhou, S., Kwon, K., 2021. Dual-Function Regeneration of Waste Lithium Cobalt Oxide for Stable High Voltage Cycle Performance. ACS Sustainable Chemistry & Engineering 9, 11194-11203. 10.1021/acssuschemeng.1c03266.

Gao, Y., Li, Y., Li, J., Xie, H., Chen, Y., 2020. Direct recovery of $LiCoO_2$ from the recycled lithium-ion batteries via structure restoration. Journal of Alloys and Compounds 845, 156234. https://doi.org/10.1016/j.jallcom.2020.156234.

Guo, Y., Li, F., Zhu, H., Li, G., Huang, J., He, W., 2016. Leaching lithium from the anode electrode materials of spent lithium-ion batteries by hydrochloric acid (HCl). Waste Management 51, 227-233. https://doi.org/10.1016/j.wasman.2015.11.036.

Jena, A., Lee, P.H., Pang, W.K., Hsiao, K.C., Peterson, V.K., Darwish, T., Yepuri, N., Wu, S.H., Chang, H., Liu, R.S., 2019. Monitoring the phase evolution in $LiCoO_2$ electrodes during battery cycles using in‐situ neutron diffraction technique. Journal of the Chinese Chemical Society 67, 344-352. 10.1002/jccs.201900448.

Lahtinen, K., Rautama, E.-L., Jiang, H., Räsänen, S., Kallio, T., 2021. Reuse of $LiCoO_2$ Electrodes Collected from Spent Li-Ion Batteries after Electrochemical Re-Lithiation of the Electrode. ChemSusChem 14, 2434-2444. https://doi.org/10.1002/cssc.202100629.

Li, L., Lu, J., Ren, Y., Zhang, X.X., Chen, R.J., Wu, F., Amine, K., 2012. Ascorbic-acid-assisted recovery of cobalt and lithium from spent Li-ion batteries. Journal of Power Sources 218, 21-27. https://doi.org/10.1016/j.jpowsour.2012.06.068.

Li, S., Wu, X., Jiang, Y., Zhou, T., Zhao, Y., Chen, X., 2021. Novel electrochemically driven and internal circulation process for valuable metals recycling from spent lithium-ion batteries. Waste Management 136, 18-27. https://doi.org/10.1016/j.wasman.2021.09.023.

Lin, J., Lin, L., Qu, S., Deng, D., Wu, Y., Yan, X., Xie, Q., Wang, L., Peng, D.L., 2021. Promising Electrode and Electrolyte Materials for High‐Energy‐Density Thin‐Film Lithium Batteries. Energy & Environmental Materials. 10.1002/eem2.12202.

Lyu, Y., Wu, X., Wang, K., Feng, Z., Cheng, T., Liu, Y., Wang, M., Chen, R., Xu, L., Zhou, J., Lu, Y., Guo, B., 2021. An Overview on the Advances of $LiCoO_2$ Cathodes for Lithium-Ion Batteries. Advanced Energy Materials 11, 2000982. https://doi.org/10.1002/aenm.202000982.

Makuza, B., Tian, Q., Guo, X., Chattopadhyay, K., Yu, D., 2021. Pyrometallurgical options for recycling spent lithium-ion batteries: A comprehensive review. Journal of Power Sources 491, 229622. 10.1016/j.jpowsour.2021.229622.

Meng, Q., Zhang, Y., Dong, P., 2018. A combined process for cobalt recovering and cathode material regeneration from spent LiCoO2 batteries: Process optimization and kinetics aspects. Waste Management 71, 372-380. https://doi.org/10.1016/j.wasman.2017.10.030.

Momma, K., Izumi, F., 2011. VESTA 3 for three-dimensional visualization of crystal, volumetric and morphology data. J. Appl. Crystallogr. 44, 1272-1276. doi:10.1107/S0021889811038970.

Moorhead-Rosenberg, Z., Allcorn, E., Manthiram, A., 2014. In Situ Mitigation of First-Cycle Anode Irreversibility in a New Spinel/FeSb Lithium-Ion Cell Enabled via a Microwave-Assisted Chemical Lithiation Process. Chemistry of Materials 26, 5905-5913. 10.1021/cm5024426.

Natarajan, S., Aravindan, V., 2018. Burgeoning Prospects of Spent Lithium-Ion Batteries in Multifarious Applications. Advanced Energy Materials 8, 1802303. https://doi.org/10.1002/aenm.201802303.

Nayaka, G.P., Zhang, Y., Dong, P., Wang, D., Zhou, Z., Duan, J., Li, X., Lin, Y., Meng, Q., Pai, K.V., Manjanna, J., Santhosh, G., 2019. An environmental friendly attempt to recycle the spent Li-ion battery cathode through organic acid leaching. Journal of Environmental Chemical Engineering 7, 102854. https://doi.org/10.1016/j.jece.2018.102854.

Nie, H., Xu, L., Song, D., Song, J., Shi, X., Wang, X., Zhang, L., Yuan, Z., 2015. $LiCoO_2$: recycling from spent batteries and regeneration with solid state synthesis. Green Chemistry 17, 1276-1280. 10.1039/C4GC01951B.

Qu, X., Xie, H., Chen, X., Tang, Y., Zhang, B., Xing, P., Yin, H., 2020. Recovery of $LiCoO_2$ from Spent Lithium-Ion Batteries through a Low-Temperature Ammonium Chloride Roasting Approach: Thermodynamics and Reaction Mechanisms. ACS Sustainable Chemistry & Engineering 8, 6524-6532. 10.1021/acssuschemeng.0c01205.

Ren, G.-x., Xiao, S.-w., Xie, M.-q., Pan, B., Chen, J., Wang, F.-g., Xia, X., 2017. Recovery of valuable metals from spent lithium ion batteries by smelting reduction process based on $FeO–SiO_2–Al_2O_3$ slag system. Transactions of Nonferrous Metals Society of China 27, 450-456. https://doi.org/10.1016/S1003-6326(17)60051-7.

Shi, S., Wang, T., Cao, M., Wang, J., Zhao, M., Yang, G., 2016. Rapid Self-Assembly Spherical $Li_{1.2}Mn_{0.56}Ni_{0.16}Co_{0.08}O_2$ with Improved Performances by Microwave Hydrothermal Method as Cathode for Lithium-Ion Batteries. ACS Applied Materials & Interfaces 8, 11476-11487. 10.1021/acsami.6b01683.

Shi, Y., Chen, G., Chen, Z., 2018. Effective regeneration of $LiCoO_2$ from spent lithium-ion batteries: a direct approach towards high-performance active particles. Green Chemistry 20, 851-862. 10.1039/C7GC02831H.

Sita, L.E., da Silva, S.P., da Silva, P.R.C., Scarminio, J., 2017. Re-synthesis of $LiCoO_2$ extracted from spent Li-ion batteries with low and high state of health. Materials Chemistry and Physics 194, 97-104. https://doi.org/10.1016/j.matchemphys.2017.03.026.

Wang, G., Wu, T., Liu, B., Gong, S., Huang, Q., Su, Y., Wu, F., Kelly, R.M., 2021. Gradient-Regeneration of $Li(Ni_{0.9}Co_{0.05}Mn_{0.05})O_2$ from Spent $LiCoO_2$ lithium-Ion Battery. Journal of The Electrochemical Society 167, 160557. 10.1149/1945-7111/abd5ff.

Wang, H., Jang, Y.I.I., Huang, B., Sadoway, D.R., Chiang, Y.M., 1999. TEM Study of Electrochemical Cycling-Induced Damage and Disorder in $LiCoO_2$ Cathodes for Rechargeable Lithium Batteries. Journal of the Electrochemical Society 146, 473-480. 10.1149/1.1391631.

Wang, S., Wang, C., Lai, F., Yan, F., Zhang, Z., 2020. Reduction-ammoniacal leaching to recycle lithium, cobalt, and nickel from spent lithium-ion batteries with a hydrothermal method: Effect of reductants and ammonium salts. Waste Management 102, 122-130. https://doi.org/10.1016/j.wasman.2019.10.017.

Wu, B., Wang, J., Li, J., Lin, W., Hu, H., Wang, F., Zhao, S., Gan, C., Zhao, J., 2016. Morphology controllable synthesis and electrochemical performance of $LiCoO_2$ for lithium-ion batteries. Electrochimica Acta 209, 315-322. https://doi.org/10.1016/j.electacta.2016.05.085.

Xue, L., Savilov, S.V., Lunin, V.V., Xia, H., 2018. Self-Standing Porous $LiCoO_2$ Nanosheet Arrays as 3D Cathodes for Flexible Li-Ion Batteries. Advanced Functional Materials 28, 1705836. https://doi.org/10.1002/adfm.201705836.

Yang, H., Deng, B., Jing, X., Li, W., Wang, D., 2021. Direct recovery of degraded $LiCoO_2$ cathode material from spent lithium-ion batteries: Efficient impurity removal toward practical applications. Waste Management 129, 85-94. https://doi.org/10.1016/j.wasman.2021.04.052.

Yang, J., Wang, W., Yang, H., Wang, D., 2020. One-pot compositional and structural regeneration of degraded $LiCoO_2$ for directly reusing it as a high-performance lithium-ion battery cathode. Green Chemistry 22, 6489-6496. 10.1039/D0GC02662J.

Yang, M., Zhou, W., Luo, F., Zhu, D., 2019a. Dielectric and microwave absorption properties of $LiCoO_2$ and its enhancement by micro-doping with metal ions. Journal of Materials Science: Materials in Electronics 30, 323-331. 10.1007/s10854-018-0296-2.

Yang, M., Zhou, W., Luo, F., Zhu, D., 2019b. Enhanced dielectric and microwave absorption properties of $LiCoO_2$ powders by magnesium doping in the X-band. Journal of the American Ceramic Society 102, 4048-4055. https://doi.org/10.1111/jace.16252.

Ye, L., Wang, C., Cao, L., Xiao, H., Zhang, J., Zhang, B., Ou, X., 2021. Effective regeneration of high-performance anode material recycled from the whole electrodes in spent lithium-ion batteries via a simplified approach. Green Energy & Environment 6, 725-733. https://doi.org/10.1016/j.gee.2020.06.017.

Yu, J., He, Y., Ge, Z., Li, H., Xie, W., Wang, S., 2018. A promising physical method for recovery of $LiCoO_2$ and graphite from spent lithium-ion batteries: Grinding flotation. Separation and Purification Technology 190, 45-52. https://doi.org/10.1016/j.seppur.2017.08.049.

Zhang, B., Xie, H., Lu, B., Chen, X., Xing, P., Qu, J., Song, Q., Yin, H., 2019a. A Green Electrochemical Process to Recover Co and Li from Spent $LiCoO_2$-Based Batteries in Molten Salts. ACS Sustainable Chemistry & Engineering 7, 13391-13399. 10.1021/acssuschemeng.9b02657.

Zhang, J., Zhang, J., Ou, X., Wang, C., Peng, C., Zhang, B., 2019b. Enhancing High-Voltage Performance of Ni-Rich Cathode by Surface Modification of Self-Assembled NASICON Fast Ionic Conductor $LiZr_2(PO_4)_3$. ACS Applied Materials & Interfaces 11, 15507-15516. 10.1021/acsami.9b00389.

Zhang, L., Xu, Z., He, Z., 2020. Electrochemical Relithiation for Direct Regeneration of $LiCoO_2$ Materials from Spent Lithium-Ion Battery Electrodes. ACS Sustainable Chemistry & Engineering 8, 11596-11605. 10.1021/acssuschemeng.0c02854.

Zhang, Z., He, W., Li, G., Xia, J., Hu, H., Huang, J., 2014. Ultrasound-assisted hydrothermal renovation of $LiCoO_2$ from the cathode of spent lithium-ion batteries. Int. J. Electrochem. Sci 9, 3691-3700.

Zhou, S., Zhang, Y., Meng, Q., Dong, P., Fei, Z., Li, Q., 2021a. Recycling of $LiCoO_2$ cathode material from spent lithium ion batteries by ultrasonic enhanced leaching and one-step regeneration. Journal of Environmental Management 277, 111426. https://doi.org/10.1016/j.jenvman.2020.111426.

Zhou, S., Zhang, Y., Meng, Q., Dong, P., Yang, X., Liu, P., Li, Q., Fei, Z., 2021b. Recycling of spent $LiCoO_2$ materials by electrolytic leaching of cathode electrode plate. Journal of Environmental Chemical Engineering 9, 104789. https://doi.org/10.1016/j.jece.2020.104789.

Zhou, Y., Shan, W., Wang, S., Lam, K.-h., Ru, Q., Chen, F., Hou, X., 2020. Recovery Li/Co from spent $LiCoO_2$ electrode based on an aqueous dual-ion lithium-air battery. Electrochimica Acta 332, 135529. https://doi.org/10.1016/j.electacta.2019.135529.

Zhu, X., Shang, K., Jiang, X., Ai, X., Yang, H., Cao, Y., 2014. Enhanced electrochemical performance of Mg-doped $LiCoO_2$ synthesized by a polymer-pyrolysis method. Ceramics International 40, 11245-11249. https://doi.org/10.1016/j.ceramint.2014.03.170.

459 Table 1 Li/Co ratio of regenerated lithium cobalt oxide under different microwave hydrothermal
460 time

Microwave hydrothermal time	Before microwave hydrothermal treatment	After microwave hydrothermal treatment	After further annealing
30 min	$Li_{0.838}CoO_2$	$Li_{0.987}CoO_2$	$Li_{0.985}CoO_2$
45 min	$Li_{0.838}CoO_2$	$Li_{1.01}CoO_2$	$Li_{0.99}CoO_2$
60 min	$Li_{0.838}CoO_2$	$Li_{1.02}CoO_2$	$Li_{1.00}CoO_2$
120 min	$Li_{0.838}CoO_2$	$Li_{1.01}CoO_2$	$Li_{1.02}CoO_2$

461

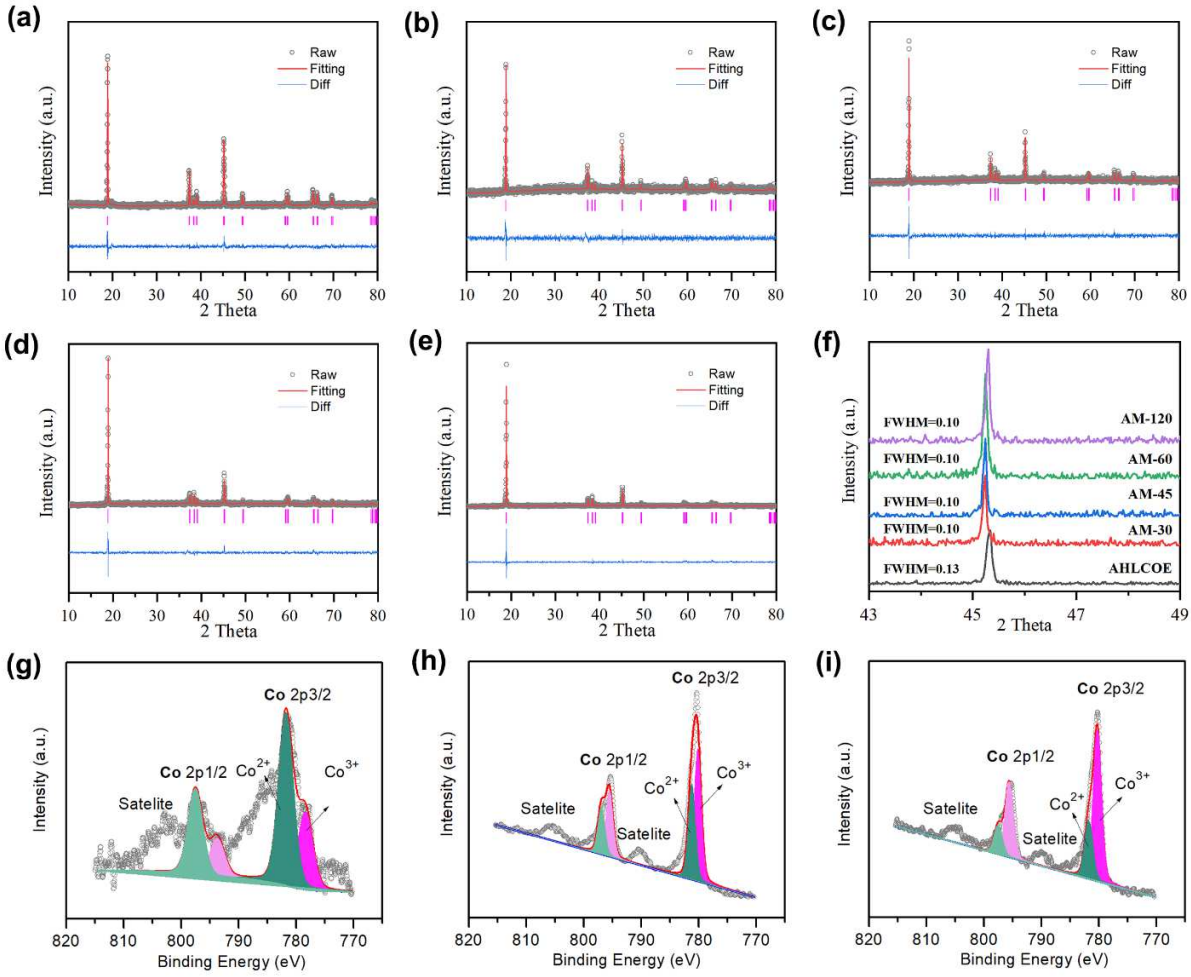

Fig. 1 XRD fitting curves of (a) AHLCOE, (b) AM-30, (c) AM-45, (d) AM-60, (e) AM-120; (f) XRD patterns of samples at 2θ of 43-49°; Co 2p XPS plots of (g) LCOE, (h) HLCOE, and (i) M-45.

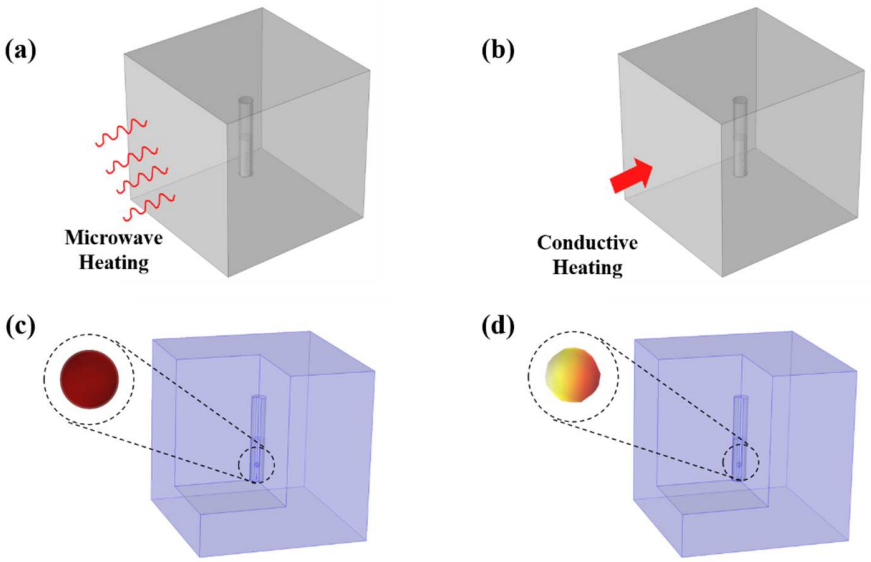

466

467 Fig. 2 Reaction model under (a) microwave heating and (b) conductive heating; estimated temperature

468 distribution of lithium cobalt oxide particle under (c) microwave heating and (d) conductive heating.

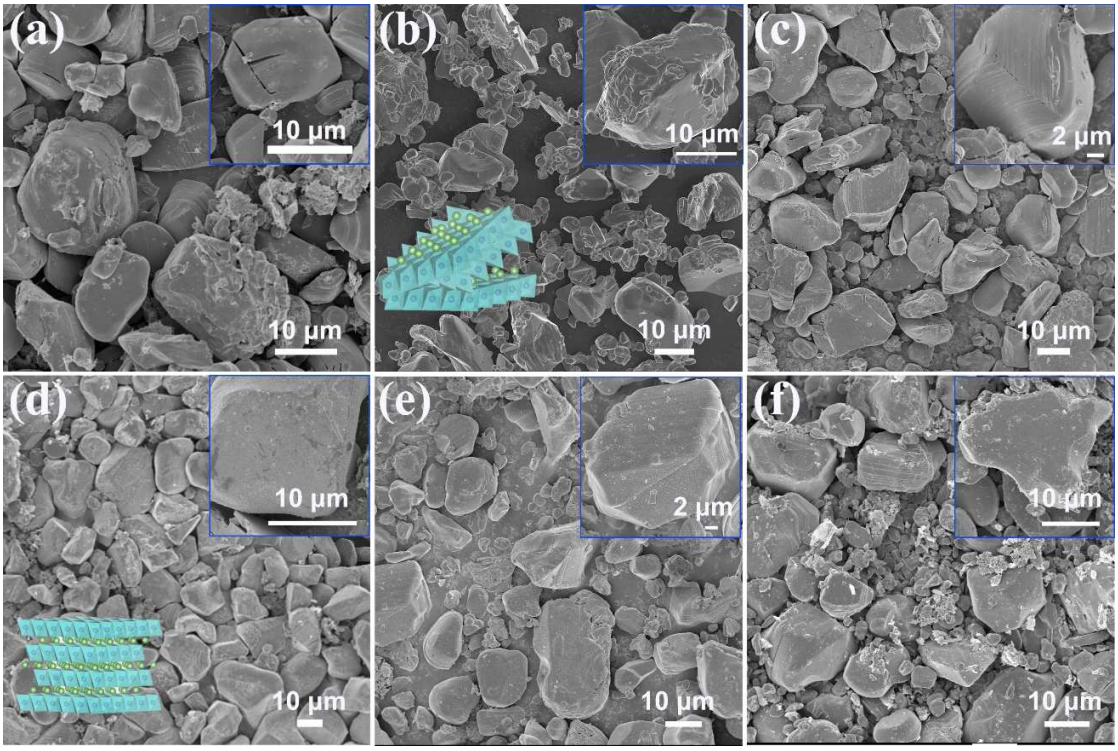

Fig. 3 SEM images: (a) LCOE, (b) AHLCOE, (c) AM-30, (d) AM-45, (e) AM-60, and (f) AM-120; insets are the magnified pictures.

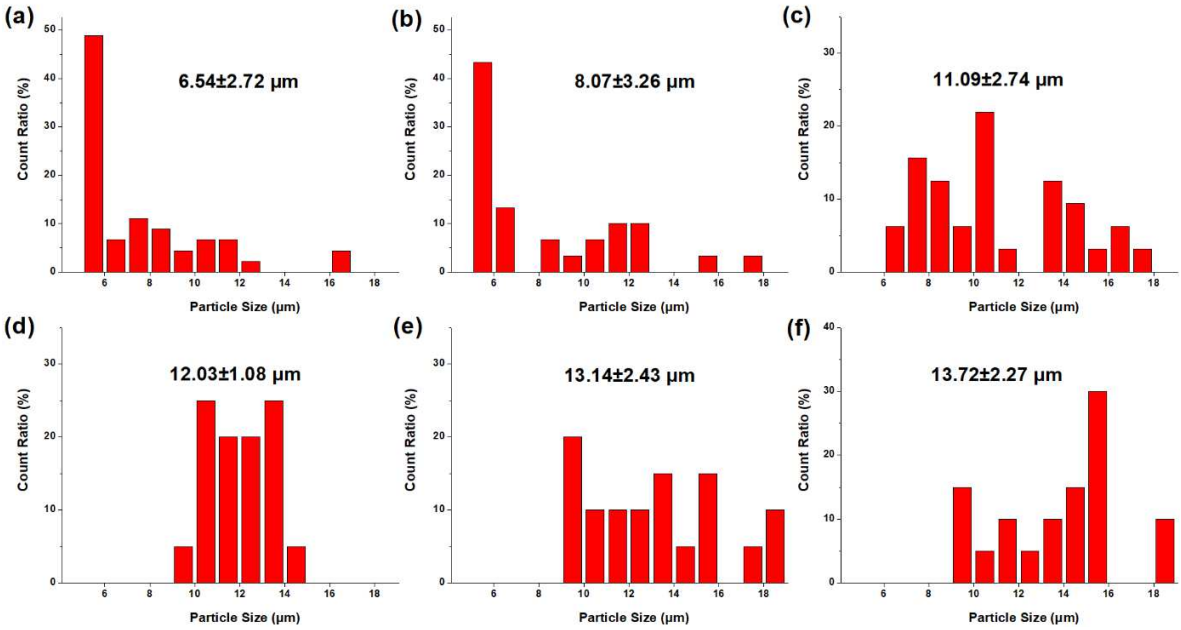

Fig. 4 Distribution of particle size: (a) LCOE, (b) AHLCOE, (c) AM-30, (d) AM-45, (e) AM-60, and (f) AM-120

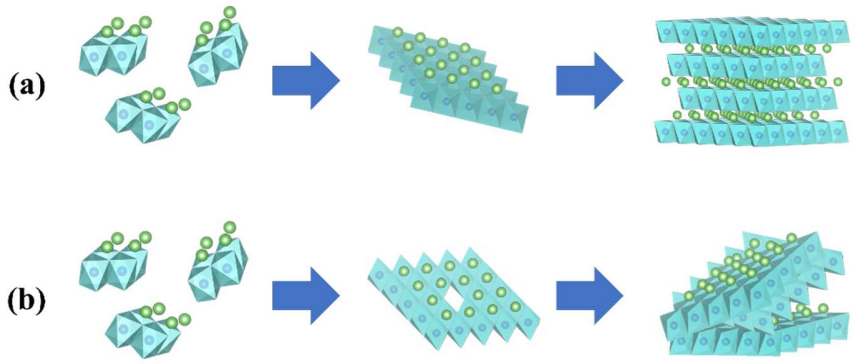

475

476 Fig. 5 Schematic for illustration of assembling $LiCoO_2$ by (a) microwave hydrothermal method

477 and (b) conventional hydrothermal method.

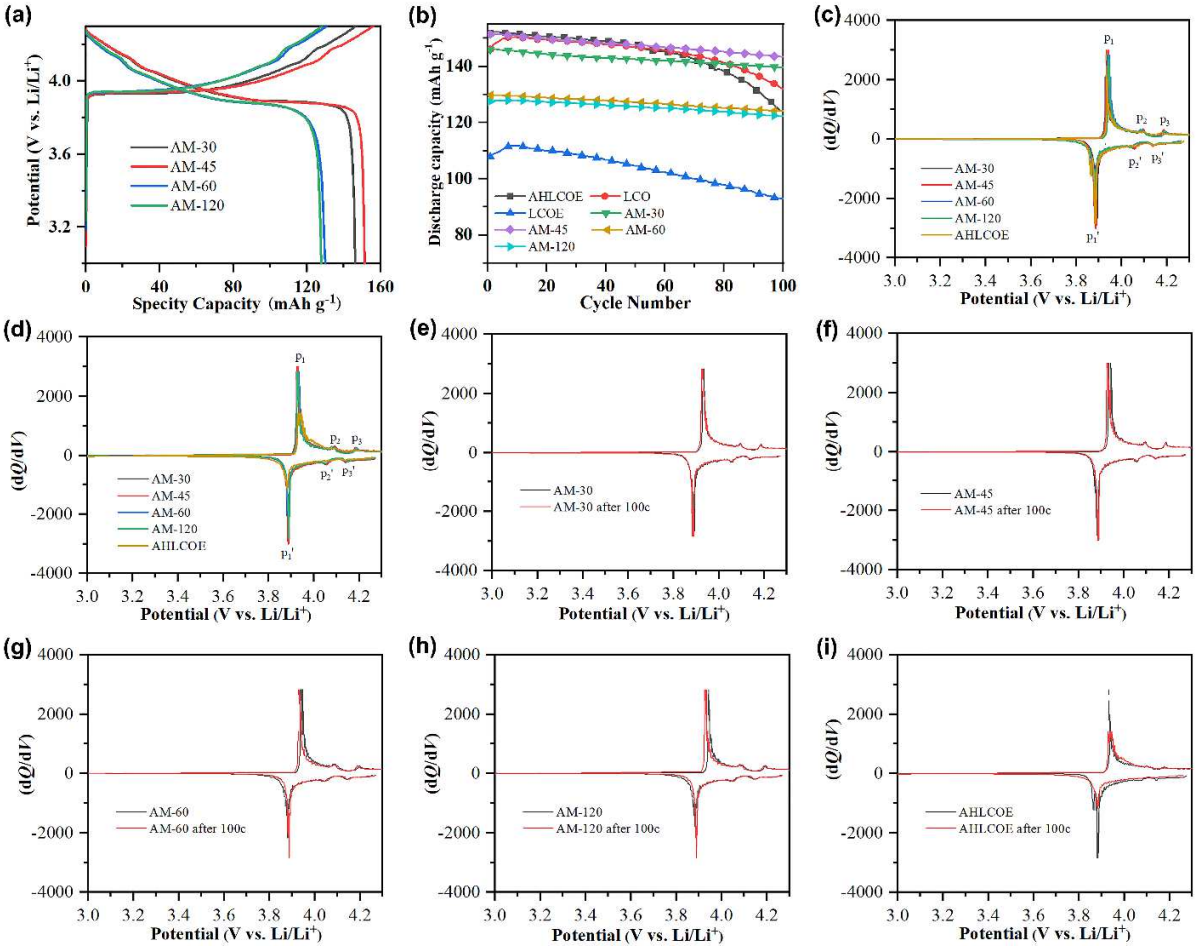

478

479 Fig. 6 (a) Charge and discharge curves of lithium cobalt oxide regenerated under different microwave

480 hydrothermal time; (b) Diagram of cycle stability for different samples, which cycles at 1 C after

481 activation for a cycle at C/10 (1 C=150 mAh g^{-1}); dQ/dV curves of samples at (c) first and (d) 100

482 cycles; dQ/dV curves of (e) AM-30, (f) AM-45, (g) AM-60, (h) AM-120, and (i) AHLCOE.

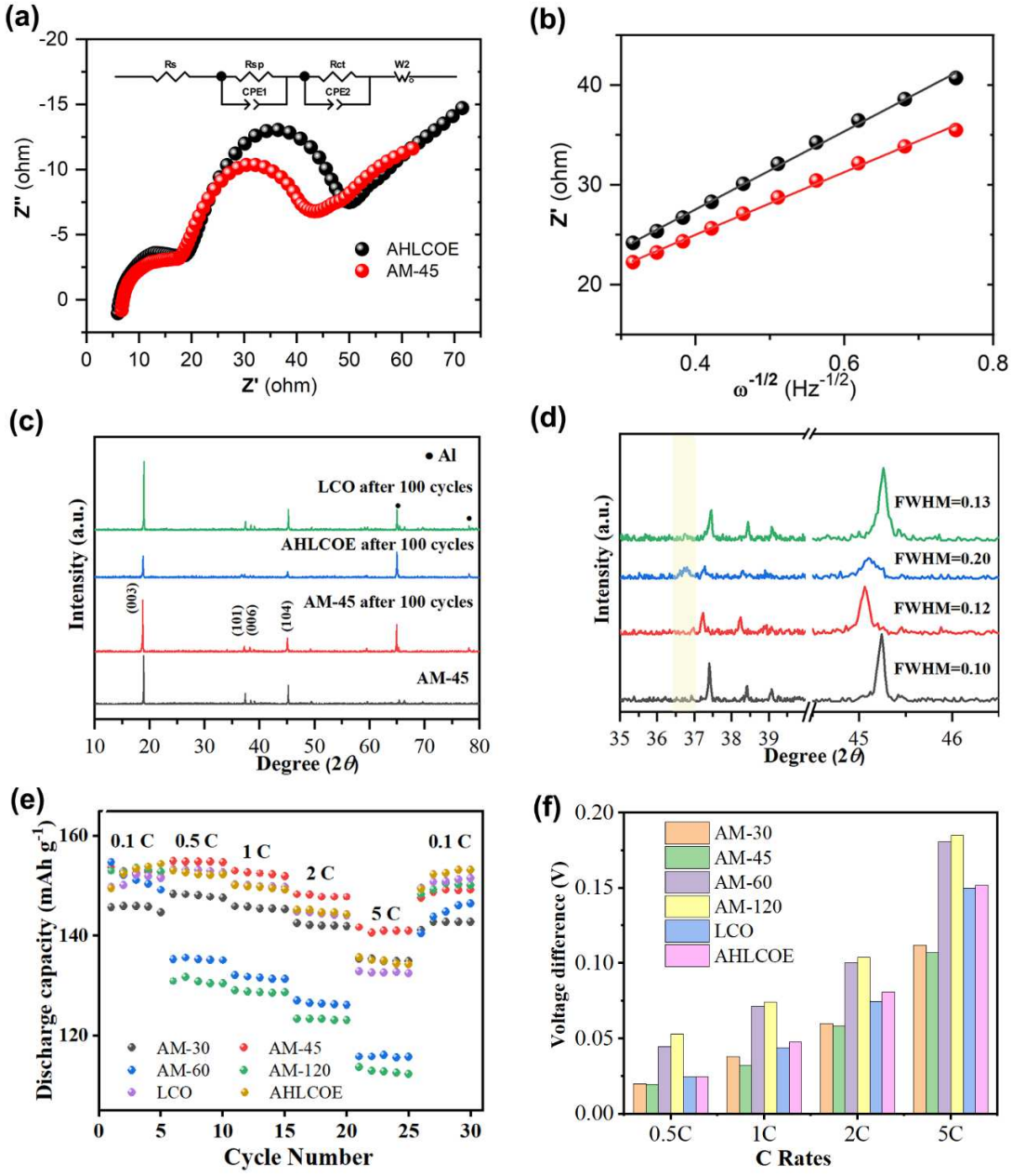

Fig. 7 (a) EIS plots and (b) the linear fitting of Z' vs $\omega^{-1/2}$ plot for AHLCOE and AM-45 after cycle tests; (c) XRD patterns and (d) partially enlarged views of samples; (e) Cycle rate performance curve and (f) the difference between the average charge and discharge voltages of samples

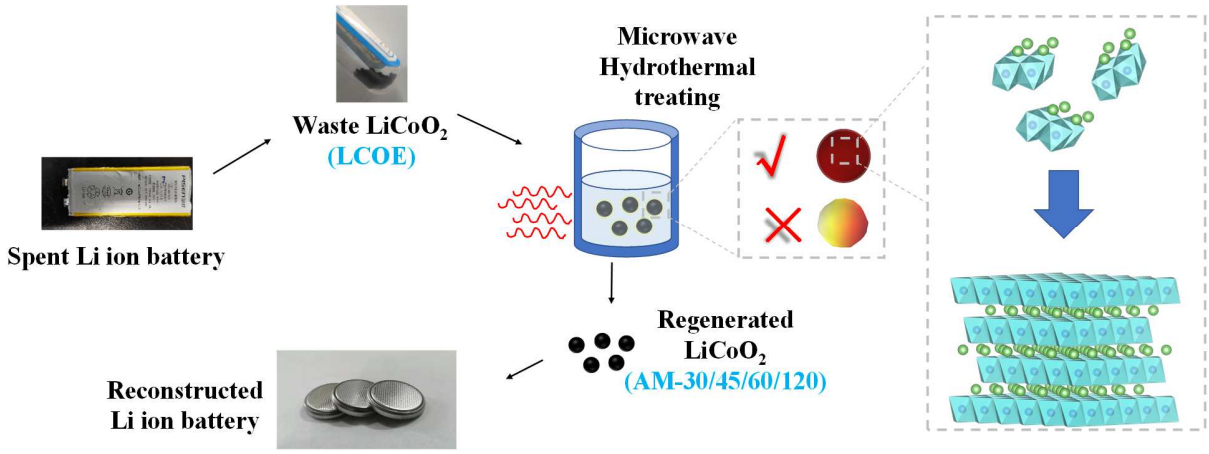

The process for constructing a high-rate and stable lithium-ion batteries from spent $LiCoO_2$ batteries.